Mechanism and Machine Theory 105 (2016) 369–387

Contents lists available at ScienceDirect

Mechanism and Machine Theory

journal homepage: www.elsevier.com/locate/mechmt

Comparison of 3-DOF asymmetrical spherical parallel manipulators with respect to motion/force transmission and stiffness

Guanglei Wu[a, b, *], Ping Zou[c]

[a] School of Mechanical Engineering, Dalian University of Technology, Dalian 116024, China
[b] Department of Mechanical and Manufacturing Engineering, Aalborg University, Aalborg 9220, Denmark
[c] School of Mechanical Engineering & Automation, Northeastern University, Shenyang 110819, China

ARTICLE INFO

Article history:
Received 7 September 2015
Received in revised form 19 July 2016
Accepted 20 July 2016
Available online 29 July 2016

Keywords:
Asymmetrical spherical parallel manipulator
Motion/force transmission
Transmission wrench screw
Stiffness
Universal joint

ABSTRACT

This paper presents a comparative study of asymmetrical spherical parallel manipulators with respect to motion/force transmission and stiffness. The manipulators adopt a center shaft to both generate a decoupled unlimited-torsion motion and support the mobile platform for high positioning accuracy, where the difference lies in the rotationally/linearly actuated limbs in-parallel. The transmission indices are defined based on the virtual coefficient between the transmission wrench and twist screws for design analysis. Comparison of the manipulators is carried out based on a multi-objective optimization approach, which aims to maximize the workspace of high transmissibility and stiffness over a regular workspace. Performance isocontours are visualized to highlight the advantages/drawbacks among the manipulator counterparts.

1. Introduction

Three degree-of-freedom (3-DOF) spherical parallel manipulators (SPMs) are intended for the applications of camera-orientating [1], minimally invasive surgical robots [2] and robotic joints [3] thanks to their large orientation workspace and high payload capacity. Typical SPMs are 3-RRR type manipulators [4–7], where R stands for revolute joint, and other types of SPMs have also been reported [8–11]. Since SPMs can generate three pure rotations, another potential application is that they can work as a tool head for complicated surface machining, where an unlimited torsion is needed in some common material processing such as milling or drilling. However, of the existing SPMs, most manipulators have a symmetrical structure, which can produce a limited torsion motion under a certain tilt orientation. In addition, the general SPMs result in low positioning accuracy [12] without a ball-and-socket joint as the center of rotation. The co-axial input SPM which has three actuation units sliding on a circular guide [13] can achieve unlimited torsion and improve the positioning accuracy, however, its unique structure leads to increased manipulator weight and inertia. To overcome the above drawbacks, an asymmetrical SPM [14] as shown in Fig. 1a is proposed with a number of advantages compared to its symmetrical counterparts. It is noted that the two actuated limb

* Corresponding author.
E-mail addresses: gwu@dlut.edu.cn (G. Wu), pzou@mail.neu.edu.cn (P. Zou).

http://dx.doi.org/10.1016/j.mechmachtheory.2016.07.017
0094-114X/

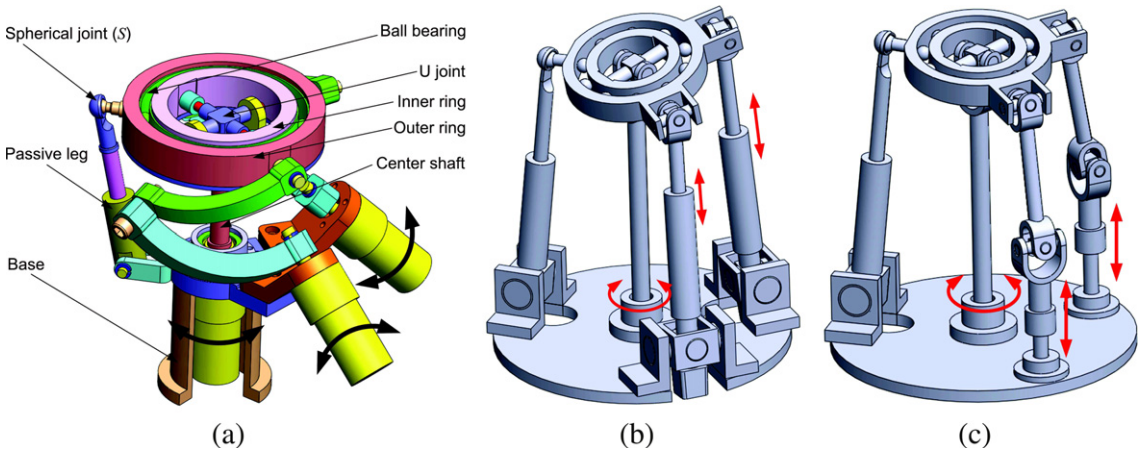

Fig. 1. Schematic of the three asymmetrical SPMs: (a) RRR; (b) UPU; (b) PUU.

in-parallel can be replaced with UPU[1] or PUU linkages as displayed in Fig. 1b and c. This paper will focus on the performance analysis and comparison of these three asymmetrical SPMs.

The principal function of mechanisms is to transmit motion/force between the input link and the output link. Therefore, the analysis of the motion/force transmission is an important concern in the design analysis of the asymmetrical SPMs, wherein a commonly adopted approach is the Jacobian analysis [15]. On the other hand, the parallel manipulators with mixed input or/and output motions, i.e., compound linear and angular motions, will result in dimensionally inhomogeneous Jacobians, thus, the performance indices of the conventional Jacobian matrix, such as condition number, may lack in physical significance [16]. In the performance evaluation, this problem can be solved by introducing a *characteristic length* [17–19] to homogenize the Jacobian matrix or the formulation of the point-based Jacobian matrices [16,20-22] by means of vertex velocity transformation of the mobile platform [23], whereas the measurements significantly depend on the choice of the *characteristic length* and the vertices. An efficient approach to accommodate this dimensional inhomogeneity is to adopt the concept of the virtual coefficient between the transmission wrench screw (TWS) and the output twist screw (OTS) introduced by Ball [24], which is closely related to the transmission/pressure angle [25–30]. For instance, Yuan et al. [31] used it as an unbounded transmission factor for spatial mechanisms. Sutherland and Roth [32] defined the transmission index using a normalized transmission factor, depending only on the linkages' geometric properties. Similarly, Chen and Angeles [33] proposed a generalized transmission index that is applicable to single-loop spatial linkages with fixed output and single or multiple DOFs. Wang et al. [34] presented the transmission analysis of fully parallel manipulators to complement the transmission indices defined by Sutherland and Roth [32] and Takeda [30]. On the basis of the quadratic singular values of the transmission matrix [23, 35], Chen et al. [36] proposed a generalized performance index for the measurement of the fully parallel manipulators. Besides, transmission analysis is also applicable for singularity identification and measurement of closeness to singularity [37, 38]. Henceforth, the virtual coefficient based indices will be adopted in this work for the analysis and evaluation of the transmission quality of the proposed manipulators.

Stiffness is another important consideration of parallel manipulators, since it is a measure of the ability of its end-effector to resist deformation due to an external wrench (forces and moments). A simple way to predict the stiffness of a manipulator is to compute its stiffness matrix [39]. Additionally, with a homogeneous stiffness matrix, stiffness can be evaluated by resorting to the eigenvalue problem [40], where the stiffness is bounded by the minimum and maximum eigenvalues of the stiffness matrix experienced in the direction of the corresponding eigenvectors. Therefore, stiffness performance have been evaluated by either minimum, maximum, average eigenvalues and/or ratio of the maximum and minimum eigenvalues of the stiffness matrix [41]. In this work, the minimum eigenvalue of the stiffness matrix is adopted as stiffness index.

This paper deals with a comparative study of three asymmetrical SPMs with respect to motion/force transmission and stiffness. The kinematic problems of the manipulators are investigated to derive their Jacobian and stiffness matrices. By virtue of the virtual coefficient between the transmission wrench and twist screws, the input and output transmission indices are defined for design analysis, of which multi-objective optimization problems are formulated to achieve the optimal design of the SPMs. The performances of the SPMs are compared to highlight the advantages/drawbacks among the manipulator counterparts.

2. Manipulators under study

Fig. 1 illustrates the three asymmetrical SPMs with identical mobile platform (MP), which is composed of an outer and inner rings connected to each other with a revolute joint, the revolute joint being realized with a revolve bearing. The orientation of

[1] Throughout this paper, R, U, S and P stand for revolute, universal, spherical and prismatic joints, respectively, and an underlined letter indicates an actuated joint.

the outer ring is determined by two RRR (UPU or PUU) limbs in parallel, respectively, and it is constrained by a fully passive RPS leg that is offset from the center of the mobile platform to eliminate the rotational motion around the vertical axis. Through a universal joint, the decoupled rotation of the inner ring is generated by the center shaft, which also supports the MP to improve the positioning accuracy. According to the kinematic linkages in parallel, the three manipulators are named as 2RRR-, 2UPU- and 2PUU-(RUR-RPS) SPMs, respectively.

The parameterizations of the three asymmetrical SPMs are depicted in Fig. 2. The reference coordinate system (x, y, z) of the 2RRR-RUR-RPS SPM is built as shown in Fig. 2a, of which the origin is located at the center of rotation, namely, point O. The z axis points upward along the vertical direction and the x axis is parallel to the segment A_1A_2 and to the axis of the revolute joint in the passive leg. The local coordinate system (X, Y, Z) attached to the outer ring is built with the origin located at point O, of which Y axis passes through the geometric center of the spherical joint in the passive leg. The ith active leg consists of three revolute joints, whose axes are parallel to unit vectors $\mathbf{u}_i$, $\mathbf{v}_i$, and $\mathbf{w}_i$. Both of these two limbs have the same architecture, defined by α_1 and α_2 angles. The base platform is defined by angles α_0 and γ, while the design parameter of the mobile platform is β.

Fig. 2b illustrates the kinematic structure of the 2UPU-RUR-RPS SPM, of which the parallel actuated limbs consist of UPU linkages. The referencecoordinate frame is attached on the base platform with the origin at the geometric center. The design parameters of the base and mobile platform are defined by an identical angle η, and h is the distance between the geometric centers of the base and mobile platforms. Moreover, the segment $\overline{A_iB_i} = l_i$, $i = 1, 2$, stands for the length of the ith active link.

Similar to Fig. 2b, the kinematic structure of the 2PUU-RUR-RPS SPM is depicted in Fig. 2c, where the difference is that the outer ring is actuated by two PUU limbs, ψ and h being the geometric parameters of the base/mobile platforms and the distance between them. Here, $\overline{A_iB_i} = d_i$ is the length of active link and the passive link has constant length $\overline{B_iC_i} = l$.

3. Kinematic analysis of the manipulators

3.1. Kinematics of 2RRR-RUR-RPS SPM

Under the prescribed coordinate system in Fig. 2a, the unit vector $\mathbf{u}_i$ is derived as:

$$\mathbf{u}_i = [\epsilon(i)\sin\alpha_0 \sin\gamma \quad \sin\alpha_0\cos\gamma - \cos\alpha_0]^T, \quad \epsilon(i) = \begin{cases} 1, & i = 1 \\ -1, & i = 2 \end{cases} \tag{1}$$

The unit vector $\mathbf{v}_i$ of the axis of the intermediate revolute joint in the ith leg is obtained in terms of the input joint angle θ_i following the angle-axis representation [14, 23], namely,

$$\mathbf{v}_i = [a_i \quad b_i \quad c_i]^T = \mathbf{R}(\mathbf{u}_i, \theta_i)\mathbf{v}_i^*; \qquad \mathbf{v}_i^* = [\epsilon(i)\sin\alpha_{01} \sin\gamma \quad \sin\alpha_{01}\cos\gamma \quad \cos\alpha_{01}]^T \tag{2}$$

where $\mathbf{v}_i^*$ is the unit vector of the axis of the intermediate revolute joint in the ith leg in its home configuration and $\alpha_{01} = \alpha_0 + \alpha_1$.

The unit vector $\mathbf{w}_i$ of the top revolute joint in the ith leg, is a function of the MP orientation:

$$\mathbf{w}_i = [x_i \quad y_i \quad z_i]^T = \mathbf{Q}\mathbf{w}_i^*; \quad \mathbf{w}_i^* = [\epsilon(i)\sin\beta \quad \cos\beta \quad 0]^T \tag{3}$$

where $\mathbf{w}_i^*$ is the unit vector of the axis of the top revolute joint of the ith leg when the mobile platform is located in its home configuration. Moreover, $\mathbf{Q} = \mathbf{R}_x(\phi_x)\mathbf{R}_y(\phi_y)$ is the rotation matrix of the outer ring. Hence, the orientation of the inner ring can be described with Cardan angles (ϕ_x, ϕ_y, ϕ_z) and its output axis is denoted by:

$$\mathbf{p} = \mathbf{Q}\mathbf{k}; \quad \mathbf{k} = [0 \quad 0 \quad 1]^T \tag{4}$$

According to the motion of the U-joint [42], the input angle θ_3 of the center shaft that is applicable to the other two manipulators is derived as:

$$\theta_3 = \tan^{-1}(\tan\phi_z \cos\phi_x \cos\phi_y) \tag{5}$$

The inverse geometric problem of the RRR leg is solved by making use of the kinematic constraints:

$$\mathbf{v}_i \cdot \mathbf{w}_i - \cos\alpha_2 = 0; \quad i = 1, 2 \tag{6}$$

whence, the input angle displacements are derived below [14]:

$$\theta_i = 2\tan^{-1}\frac{-I_i \pm \sqrt{I_i^2 + J_i^2 - K_i^2}}{K_i - J_i} \tag{7}$$

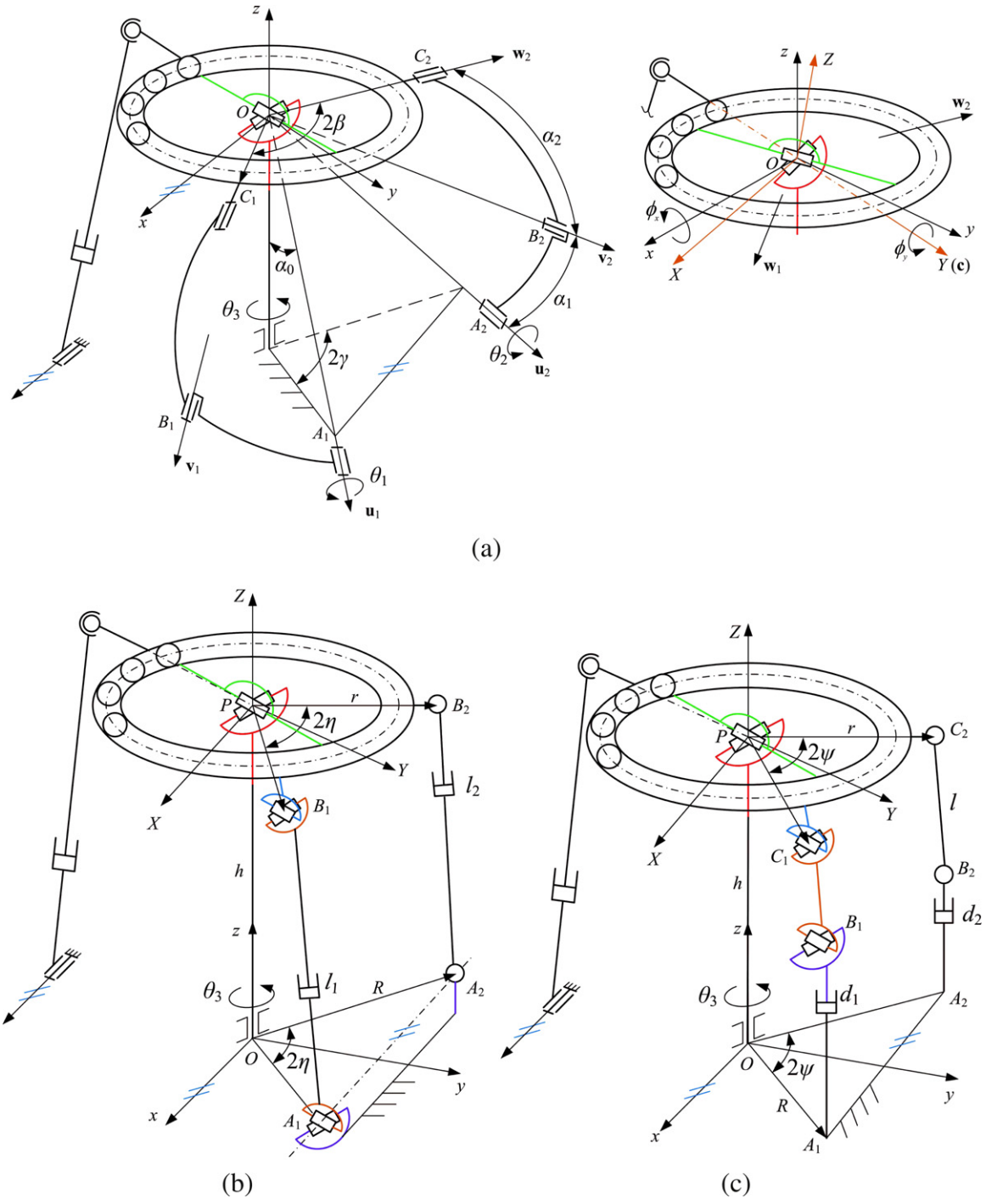

Fig. 2. Parameterizations of the asymmetrical SPMs: (a) RRR; (b) UPU; (c) PUU.

with

$$I_i = (x_i c\gamma - \epsilon(i) y_i s\gamma) s\alpha_1 \tag{8a}$$

$$J_i = (\epsilon(i) x_i c\alpha_0 s\gamma + y_i c\alpha_0 c\gamma + z_i s\alpha_0) s\alpha_1 \tag{8b}$$

$$K_i = (\epsilon(i) x_i s\alpha_0 s\gamma + y_i s\alpha_0 c\gamma - z_i c\alpha_0) s\alpha_1 - c\alpha_2 \tag{8c}$$

where s and c stand for the sine and cosine functions, respectively.

Differentiating Eqs. (6) and (5) with respect to time leads to

$$\begin{bmatrix} A_{11} & A_{12} & 0 \\ A_{21} & A_{22} & 0 \\ A_{31} & A_{32} & A_{33} \end{bmatrix} \begin{bmatrix} \dot{\phi}_x \\ \dot{\phi}_y \\ \dot{\phi}_z \end{bmatrix} = \begin{bmatrix} B_{11} & 0 & 0 \\ 0 & B_{22} & 0 \\ 0 & 0 & B_{33} \end{bmatrix} \begin{bmatrix} \dot{\theta}_1 \\ \dot{\theta}_2 \\ \dot{\theta}_3 \end{bmatrix} \quad \text{or} \quad \mathbf{A}\dot{\boldsymbol{\phi}} = \mathbf{B}\dot{\boldsymbol{\theta}} \tag{9}$$

with

$$A_{i1} = b_i(\epsilon(i)\mathrm{c}\phi_x\mathrm{s}\phi_y\mathrm{s}\beta - \mathrm{s}\phi_x\mathrm{c}\beta) + c_i(-\epsilon(i)\mathrm{s}\phi_x\mathrm{s}\phi_y\mathrm{s}\beta + \mathrm{c}\phi_x\mathrm{c}\beta), \quad i = 1,\ 2 \tag{10a}$$

$$A_{i2} = -\epsilon(i)a_i\mathrm{s}\phi_y\mathrm{s}\beta + \epsilon(i)b_i\mathrm{s}\phi_x\mathrm{c}\phi_y\mathrm{s}\beta - \epsilon(i)c_i\mathrm{c}\phi_x\mathrm{c}\phi_y\mathrm{s}\beta, \quad i = 1,\ 2 \tag{10b}$$

$$B_{ii} = x_i\mathrm{s}\alpha_1(\mathrm{s}\theta_i\mathrm{s}\gamma\mathrm{c}\alpha_0 - \epsilon(i)\mathrm{c}\theta_i\mathrm{c}\gamma) + y_i\mathrm{s}\alpha_1(\mathrm{s}\theta_i\mathrm{c}\gamma\mathrm{c}\alpha_0 + \epsilon(i)\mathrm{c}\theta_i\mathrm{s}\gamma) + c_i\mathrm{s}\theta_i\mathrm{s}\alpha_0\mathrm{s}\alpha_1, \quad i = 1,\ 2 \tag{10c}$$

$$A_{31} = \sin\phi_x\cos\phi_y\tan\phi_z,\ A_{32} = \mathrm{c}\phi_x\mathrm{s}\phi_y\tan\phi_z,\ A_{33} = -\mathrm{c}\phi_x\mathrm{c}\phi_y(1+\tan^2\phi_z),\ B_{33} = 1+\tan^2\theta_3 \tag{10d}$$

To this end, the kinematic Jacobian matrix of the manipulator is expressed as

$$\mathbf{J} = \boldsymbol{\Phi}\mathbf{A}^{-1}\mathbf{B}; \quad \boldsymbol{\Phi} = \begin{bmatrix} \cos\phi_x\cos\phi_z & \sin\phi_z & 0 \\ -\cos\phi_y\sin\phi_z & \cos\phi_z & 0 \\ \sin\phi_y & 0 & 1 \end{bmatrix} \tag{11}$$

where $\boldsymbol{\Phi}$, derived from the time derivative of Euler convention $X--Y--Z$ [43], is the transformation matrix between the Euler angle rates and angular velocities.

3.2. Kinematics of 2UPU-RUR-RPS SPM

From Fig. 2b, the inverse geometric problem for the ith leg is computed as

$$l_i = \parallel \mathbf{b}_i - \mathbf{a}_i \parallel; \quad i = 1,\ 2 \tag{12}$$

where

$$\mathbf{b}_i = r\mathbf{Q}\mathbf{e}_i + h\mathbf{k}, \quad \mathbf{a}_i = R\mathbf{e}_i; \quad \mathbf{e}_i = [\epsilon(i)\sin\eta \quad \cos\eta \quad 0] \tag{13}$$

The Jacobian matrix is deduced upon the differentiation of the kinematic constraint equations with respect to time, where the different elements in comparison with Eq. (9) are expressed as:

$$A_{i1} = -Rrc\eta(c\eta s\phi_x - \epsilon(i)s\eta c\phi_x s\phi_y) + hr(-\epsilon(i)s\eta s\phi_x s\phi_y - c\eta c\phi_x), \quad i = 1,\ 2 \tag{14a}$$

$$A_{i2} = rs\eta(-Rs\eta s\phi_y + \epsilon(i)hc\phi_x c\phi_y + \epsilon(i)Rc\eta s\phi_x c\phi_y), \quad i = 1,\ 2 \tag{14b}$$

$$B_{ii} = -l_i, \quad i = 1,\ 2 \tag{14c}$$

Consequently, the kinematic Jacobian matrix takes the same form as expressed in Eq. (11).

3.3. Kinematics of 2PUU-RUR-RPS SPM

In accordance with Fig. 2c, the inverse geometric problem is solved by making use of the following closed-loop equation:

$$\parallel \mathbf{c}_i - \mathbf{b}_i \parallel - l = 0; \quad i = 1,\ 2 \tag{15}$$

where $\mathbf{c}_i$ and $\mathbf{b}_i$, respectively, are the Cartesian coordinates of points C_i and B_i, namely,

$$\mathbf{c}_i = r\mathbf{Q}\mathbf{h}_i + h\mathbf{k}, \quad \mathbf{b}_i = R\mathbf{h}_i + d_i\mathbf{k}; \quad \mathbf{h}_i = [\epsilon(i)\sin\psi \quad \cos\psi \quad 0] \tag{16}$$

Subsequently, the inverse geometric problem is derived as

$$d_i = h + rc\psi s\phi_x - \epsilon(i)rs\psi c\phi_x s\phi_y - \sqrt{l^2 - (\epsilon(i)rc\psi c\phi_x + rs\psi s\phi_x s\phi_y - Rc\psi)^2 - (rs\psi c\phi_y - Rs\psi)^2} \tag{17}$$

By the same token, the Jacobian matrix can be derived from the kinematic constraint equations, where the elements in matrices **A** and **B** are given by

$$A_{i1} = Rrc\psi(c\psi s\phi_x - \epsilon(i)s\psi c\phi_x s\phi_y) + r(h - d_i)(\epsilon(i)s\psi s\phi_x s\phi_y + c\psi c\phi_x), \quad i = 1,\ 2 \tag{18a}$$

$$A_{i2} = Rrs\psi(s\psi s\phi_y - \epsilon(i)c\psi s\phi_x c\phi_y) - \epsilon(i)r(h - d_i)s\psi c\phi_x c\phi_y, \quad i = 1,\ 2 \tag{18b}$$

$$B_{ii} = h - d_i + rc\psi s\phi_x - \epsilon(i)rs\psi c\phi_x s\phi_y, \quad i = 1,\ 2 \tag{18c}$$

4. Stiffness matrix of the SPMs

Of the existing methods, the Virtual Joint Method (VJM) [44–48], which is often called lumped modeling, is widely used to establish the stiffness model for parallel manipulators (PMs), as it provides acceptable accuracy in short computational time. Here, the assumption is made by ignoring the structural compliance and the influence of external wrench, thus, the stiffness matrix of the asymmetrical SPM is derived as below

$$\mathbf{K} = \mathbf{J}^{-T}\mathbf{K}_{\text{act}}\ \ \mathbf{J}^{-1} \tag{19}$$

where **J** is the foregoing derived Jacobian matrix and $\mathbf{K}_{\text{act}} = \text{diag}[k_{12}\ k_{12}\ k_{\theta 3}]$ is the stiffness matrix in the joint space. Here, $k_{12} = k_\theta$ stands for the stiffness of the rotational actuated joint in the RRR limb, while $k_{12} = k_\rho$ stands for that of linear actuated joint in the UPU or PUU limb. Moreover, $k_{\theta 3}$ denotes the rotational stiffness of the center shaft.

5. Transmission index

The main function of the mechanism is to transmit motion/force between the input link and the output one. In order to evaluate the transmission performance of the manipulator, some transmission indices (TI) need to be defined. Here, the virtual coefficient based indices [33] is adopted for the evaluation of the transmission quality.

5.1. Transmission wrench and twist screw

As depicted in Fig. 3, the instantaneous motion of a rigid body can be represented by using a twist screw defined by its Plücker coordinates:

$$\$_T = (\boldsymbol{\omega}\ ;\ \mathbf{v}) = (\omega\mathbf{e}_1\ ;\ \omega\mathbf{r}_1 \times \mathbf{e}_1 + v\mathbf{e}_1) = \omega(\mathbf{e}_1\ ;\ \mathbf{r}_1 \times \mathbf{e}_1 + p_1\mathbf{e}_1) = \omega\hat{\$}_T \tag{20}$$

where vectors $\mathbf{e}_1$ and $\mathbf{r}_1$ denote the direction of and a point on the twist axis, respectively, scalars ω and v are the magnitude of angular velocity and partial linear velocity along the axis, and p_1 is defined as the pitch, i.e., the ratio of the linear velocity to angular velocity $p_1 = v/\omega$. Moreover, in $\$_T = \omega\hat{\$}_T$, ω is the amplitude of the twist screw and $\hat{\$}_T$ stands for the unit twist screw.

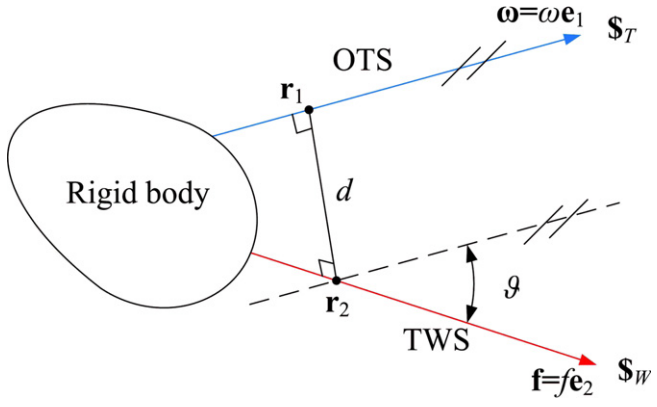

Fig. 3. The twist screw and transmission wrench screw of a rigid body.

Likewise, a wrench exerted on the rigid body can be expressed as a wrench screw defined by its Plücker coordinates below:

$$\$_W = (\mathbf{f}\ ;\ \mathbf{m}) = (f\mathbf{e}_2\ ;\ f\mathbf{r}_2 \times \mathbf{e}_2 + m\mathbf{e}_2) = f(\mathbf{e}_2\ ;\ \mathbf{r}_2 \times \mathbf{e}_2 + p_2\mathbf{e}_2) = f\hat{\$}_W \tag{21}$$

where vectors $\mathbf{e}_2$ and $\mathbf{r}_2$ are the direction of and a point on the wrench axis, respectively, scalars f and m are magnitude of the force and partial moment along the axis, coupled by a pitch $p_2 = m/f$. Moreover, in $\$_W = f\hat{\$}_W$, f is the amplitude of the wrench screw and $\hat{\$}_W$ is the unit wrench screw.

The reciprocal product between the twist $\$_T$ and wrench $\$_W$ screws is defined as:

$$\$_T \circ \$_W = \mathbf{f}\cdot\mathbf{v} + \mathbf{m}\cdot\boldsymbol{\omega} = \omega f\hat{\$}_T \circ \hat{\$}_W \tag{22}$$

This reciprocal product amounts to the instantaneous power between the wrench and the twist screws [49]. The product $\hat{\$}_T \circ \hat{\$}_W$ is equal to

$$\hat{\$}_T \circ \hat{\$}_W = (p_1 + p_2)\mathbf{e}_1^T\mathbf{e}_2 + (\mathbf{r}_1 - \mathbf{r}_2)^T(\mathbf{e}_1 \times \mathbf{e}_2) = (p_1 + p_2)\cos\vartheta - d\sin\vartheta \tag{23}$$

where d and ϑ are the distance and the angle between the two screw axes, respectively. With the given twist and wrench, their pitches p_1 and p_2, are considered to be constant, thus, the maximal magnitude of the reciprocal product of $\hat{\$}_T$ and $\hat{\$}_W$ being

$$|\hat{\$}_T \circ \hat{\$}_W|_{\max} = \sqrt{(p_1 + p_2)^2 + d_{\max}^2} \tag{24}$$

where $d_{\max}$ denotes the maximal distance between the two screw axes [34]. Subsequently, the transmission index is defined as a dimensionless index [32, 33], bounded by 0 and 1:

$$\mathrm{TI} = \frac{|\hat{\$}_T \circ \hat{\$}_W|}{|\hat{\$}_T \circ \hat{\$}_W|_{\max}} \tag{25}$$

where $|\hat{\$}_T \circ \hat{\$}_W|_{\max}$ represents the potential maximal magnitude of the reciprocal product between $\hat{\$}_T$ and $\hat{\$}_W$. The larger TI, the more important the power transmission from the wrench to the twist, namely, the better the transmission quality.

It is noteworthy that, as special cases of twist screw, a pure rotation and a pure translation in space are represented by a twist of zero pitch and infinite pitch, respectively, written as,

$$\$_T = \begin{cases} \omega\hat{\$}_T = \omega(\mathbf{e}_1\ ;\ \mathbf{r}_1 \times \mathbf{e}_1); & p_1 = 0,\ \text{pure rotation} \\ v\hat{\$}_T = v(\mathbf{0}\ ;\ \mathbf{e}_1); & p_1 = \infty,\ \text{pure translation} \end{cases} \tag{26}$$

Similarly, a pure force and a pure couple (or moment) are represented by a wrench of zero pitch and infinite pitch, respectively, written as,

$$\$_W = \begin{cases} f\hat{\$}_W = f(\mathbf{e}_2\ ;\ \mathbf{r}_2 \times \mathbf{e}_2); & p_2 = 0,\ \text{pure force} \\ m\hat{\$}_W = m(\mathbf{0}\ ;\ \mathbf{e}_2); & p_2 = \infty,\ \text{pure couple} \end{cases} \tag{27}$$

5.2. Input transmission index

For the robot linkage, the motion is transmitted from the input link to the output one. As a result, the force applied to the output link is to be transmitted to the input one. The internal wrench arising due to the transmission is called the transmission wrench [33], which can be expressed by the transmission wrench screw (TWS). In order to evaluate the input transmission performance, the power coefficient between the TWS and the input twist screw is defined as its input transmission index (ITI).

5.2.1. ITI of RRR limb

The wrench applied to a SPM is usually a pure moment, thus, for a spherical RRR leg, the transmission wrench is a pure torque. As the TWS is reciprocal to all the passive joint screws in the leg, the axis of the wrench in the ith leg is perpendicular to the plane OB_iC_i and passes through point O, as shown in Fig. 4a. In accordance with Eq. (25), the input transmission index of the ith RRR leg is defined as [14, 34]:

$$\lambda_{Ii} = \frac{|\hat{\$}_{Ii} \circ \hat{\$}_{Wi}|}{|\hat{\$}_{Ii} \circ \hat{\$}_{Wi}|_{\max}} = \frac{|\mathbf{u}_i \cdot \boldsymbol{\tau}_i|}{|\mathbf{u}_i \cdot \boldsymbol{\tau}_i|_{\max}}, \quad i = 1,\ 2 \tag{28}$$

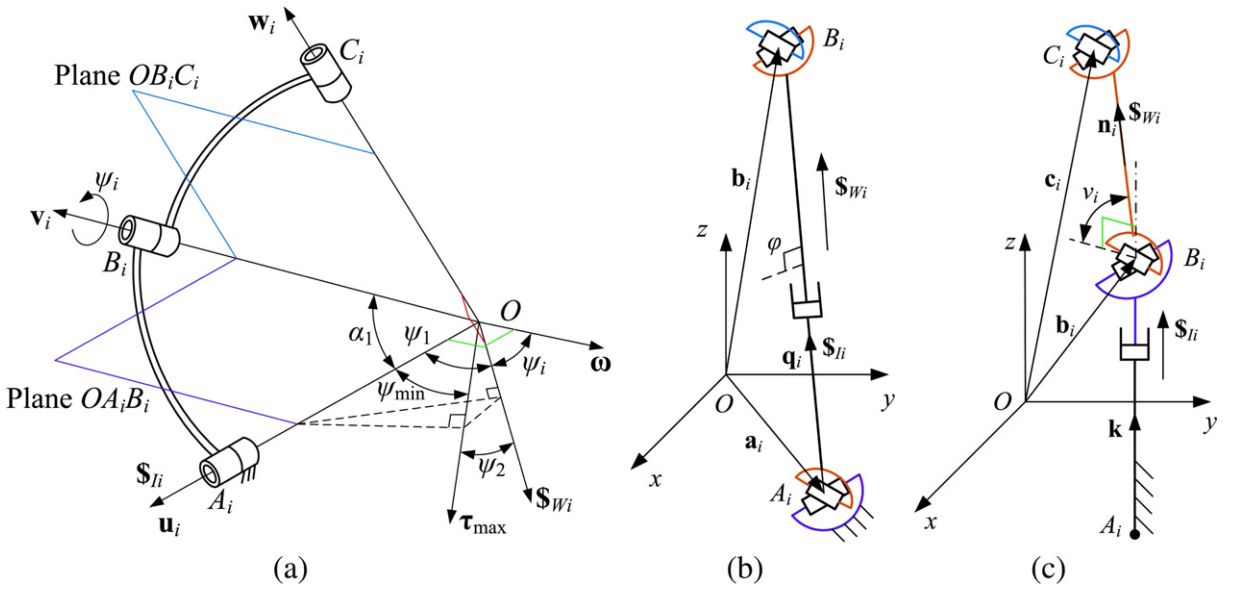

Fig. 4. The input twist screw and transmission wrench screw of kinematic linkages: (a) RRR limb; (b) UPU limb; (c) PUU limb.

with

$$\hat{\$}_{Ii} = \begin{bmatrix} \mathbf{u}_i \\ \mathbf{0} \end{bmatrix}; \quad \hat{\$}_{Wi} = \begin{bmatrix} \mathbf{0} \\ \boldsymbol{\tau}_i \end{bmatrix}, \quad \boldsymbol{\tau}_i = \frac{\mathbf{v}_i \times \mathbf{w}_i}{\| \mathbf{v}_i \times \mathbf{w}_i \|} \tag{29}$$

Based upon the geometry in Fig. 4a, one obtains

$$|\mathbf{u}_i \cdot \boldsymbol{\tau}_i|_{\max} = |\mathbf{u}_i \cdot \boldsymbol{\tau}_{\max}| = |\cos\psi_{\min}| = |\sin\alpha_1| \tag{30}$$

which means that $|\mathbf{u}_i \cdot \boldsymbol{\tau}_i|$ reaches its maximum when $\hat{\$}_{Wi}$ lies in the plane OA_iB_i, namely, plane OB_iC_i being perpendicular to plane OA_iB_i. Eq. (28) can be written as

$$\lambda_{Ii} = \frac{|\cos\psi_1|}{|\cos\psi_{\min}|} = |\cos\psi_2| = |\sin\psi_i| = \sqrt{1-\cos^2\psi_i} \tag{31}$$

where ψ_i is the input transmission angle, corresponding to the motion transmission in the ith limb, i.e., the angle between planes OA_iB_i and OB_iC_i:

$$\cos\psi_i = \frac{(\mathbf{v}_i \times \mathbf{u}_i)\cdot(\mathbf{v}_i \times \mathbf{w}_i)}{\| \mathbf{v}_i \times \mathbf{u}_i \| \| \mathbf{v}_i \times \mathbf{w}_i \|} \tag{32}$$

5.2.2. ITI of UPU limb

For a UPU limb depicted in Fig. 4b, since the input twist is a translation, the pitch of the input twist screw is infinite [34]. The unit input twist screw $\hat{\$}_{Ii}$ and TWS $\hat{\$}_{Wi}$ of the ith limb can be expressed as

$$\hat{\$}_{Ii} = \begin{bmatrix} \mathbf{0} \\ \mathbf{q}_i \end{bmatrix}, \quad \mathbf{q}_i = \frac{\mathbf{b}_i - \mathbf{a}_i}{\| \mathbf{b}_i - \mathbf{a}_i \|}; \quad \hat{\$}_{Wi} = \begin{bmatrix} \mathbf{q}_i \\ \mathbf{b}_i \times \mathbf{q}_i \end{bmatrix} \tag{33}$$

As a result, the input transmission index of the UPU limb is a constant, i.e., $\mu_{I1} = \mu_{I2} = sin\varphi = 1$.

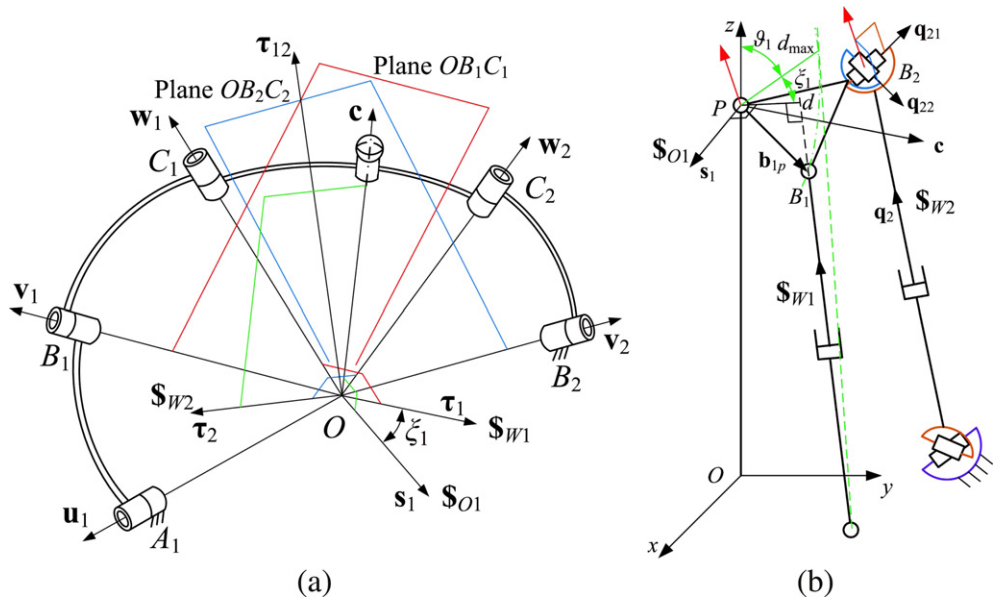

Fig. 5. The output twist screw and transmission wrench screw of kinematic linkages: (a) RRR limb; (b) UPU limb.

5.2.3. ITI of PUU limb

Similar to the UPU limb, the pitch of the input twist screw of the PUU limb is infinite [34]. The unit input twist screw $\hat{\mathbf{S}}_{Ii}$ with and TWS $\hat{\mathbf{S}}_{Wi}$ of the ith limb can be expressed as

$$\hat{\mathbf{S}}_{Ii} = \begin{bmatrix} \mathbf{0} \\ \mathbf{k} \end{bmatrix}; \quad \hat{\mathbf{S}}_{Wi} = \begin{bmatrix} \mathbf{n}_i \\ \mathbf{c}_i \times \mathbf{n}_i \end{bmatrix}, \quad \mathbf{n}_i = \frac{\mathbf{c}_i - \mathbf{b}_i}{\| \mathbf{c}_i - \mathbf{b}_i \|} \tag{34}$$

Referring to Eq. (25), the input transmission index of the ith PUU leg is calculated as:

$$\rho_{Ii} = \frac{|\hat{\mathbf{S}}_{Ii} \circ \hat{\mathbf{S}}_{Wi}|}{|\hat{\mathbf{S}}_{Ii} \circ \hat{\mathbf{S}}_{Wi}|_{\max}} = \frac{|\mathbf{k} \cdot \mathbf{n}_i|}{|\mathbf{k} \cdot \mathbf{n}_i|_{\max}} = \sin \nu_i, \quad i = 1,\ 2 \tag{35}$$

where ν_i is the transmission angle, i.e., the angle between the normal to the actuation line in the plane OA_iB_i and $\mathbf{n}_i$ of the force line.

5.3. Output transmission index

The output transmission index (OTI) is defined by referring to the pressure angle at the attached point of the leg with the moving platform [30]. The OTI of a single leg is obtained by the method of fixing the other input joints [34], where the parallel manipulator thus becomes a 1-DOF system. Subsequently, the power coefficient between the TWS and the output twist screw (OTS) is defined as the output transmission index (OTI).

5.3.1. OTI of RRR SPM

By fixing the active joint at point A_2 (point B_2 will be fixed) while keeping joint at point A_1 actuated as shown in Fig. 5a, the transmission wrench $\boldsymbol{\$}_{W2}$ becomes a constraint wrench to the mobile platform. The instantaneous motion of the mobile platform will be a rotation about a unique vector constrained by $\boldsymbol{\$}_{W2}$ and the vector $\mathbf{c}$ in the passive leg [14], namely,

$$\mathbf{s}_1 = \frac{\boldsymbol{\tau}_2 \times \mathbf{c}}{\| \boldsymbol{\tau}_2 \times \mathbf{c} \|}; \quad \mathbf{c} = \mathbf{Q} \cdot [0 \quad 1 \quad 0]^T \tag{36}$$

Thus, the output twist screw of the first limb can be expressed as: $\hat{\mathbf{S}}_{O1} = (\mathbf{s}_1;\ \mathbf{0})$. Based on Eq. (25), the output transmission index of the first limb is defined by

$$\lambda_{O1} = \frac{|\hat{\mathbf{S}}_{O1} \circ \hat{\mathbf{S}}_{W1}|}{|\hat{\mathbf{S}}_{O1} \circ \hat{\mathbf{S}}_{W1}|_{\max}} = \frac{|\mathbf{s}_1 \cdot \boldsymbol{\tau}_1|}{|\mathbf{s}_1 \cdot \boldsymbol{\tau}_1|_{\max}} = |\mathbf{s}_1 \cdot \boldsymbol{\tau}_1| = \cos \varepsilon_1 \tag{37}$$

Eq. (37) can be rewritten as

$$\lambda_{O1} = \frac{|\boldsymbol{\tau}_2 \times \mathbf{c} \cdot \boldsymbol{\tau}_1|}{\| \boldsymbol{\tau}_2 \times \mathbf{c} \|} = \frac{|\boldsymbol{\tau}_{12} \cdot \mathbf{c}|}{\| \boldsymbol{\tau}_2 \times \mathbf{c} \|}; \quad \boldsymbol{\tau}_{12} = \boldsymbol{\tau}_1 \times \boldsymbol{\tau}_2 \tag{38}$$

By the same token, the output transmission index of the second limb is derived as:

$$\lambda_{O2} = \frac{|\boldsymbol{\tau}_{12} \cdot \mathbf{c}|}{\| \boldsymbol{\tau}_1 \times \mathbf{c} \|} \tag{39}$$

5.3.2. OTI of UPU SPM

For the UPU SPM, as displayed in Fig. 5b, when the active prismatic joint in the second limb is locked, the instantaneous axis of rotation of the platform will be parallel to the unit vector below

$$\mathbf{s}_1 = \frac{\mathbf{q}_{21} \times \mathbf{q}_{22} \times \mathbf{c}}{\| \mathbf{q}_{21} \times \mathbf{q}_{22} \times \mathbf{c} \|}; \quad \mathbf{q}_{22} = \mathbf{QEe}_2, \quad \mathbf{q}_{21} = \frac{\mathbf{Ee}_2 \times \mathbf{q}_2}{\| \mathbf{Ee}_2 \times \mathbf{q}_2 \|} \tag{40}$$

where $\mathbf{E} = \mathbf{R}_z(\pi/2)$. Thus, the output twist screw (OTS) of the first limb is obtained as:

$$\hat{\mathbf{S}}_{O1} = \begin{bmatrix} \mathbf{s}_1 \\ \mathbf{s}_1 \times \mathbf{b}_{1p} \end{bmatrix} = \begin{bmatrix} \mathbf{s}_1 \\ r\mathbf{s}_1 \times \mathbf{Qe}_1 \end{bmatrix} \tag{41}$$

On the basis of Eq. (25), the OTI of the first limb is expressed as:

$$\mu_{O1} = \frac{|\hat{\mathbf{S}}_{O1} \circ \hat{\mathbf{S}}_{W1}|}{|\hat{\mathbf{S}}_{O1} \circ \hat{\mathbf{S}}_{W1}|_{\max}} = \frac{|(2r\mathbf{Qe}_1 + h\mathbf{k}) \cdot \mathbf{q}_1 \times \mathbf{s}_1|}{|(2r\mathbf{Qe}_1 + h\mathbf{k}) \cdot \mathbf{q}_1 \times \mathbf{s}_1|_{\max}} \tag{42}$$

When $\mathbf{s}_1$ is perpendicular to the plane determined by vectors $\mathbf{Qe}_1$ and $\mathbf{s}_1$, $|\hat{\mathbf{S}}_{O1} \circ \hat{\mathbf{S}}_{W1}|$ is a maximum. As the OTS is a pure rotation and TWS is a pure force, the pitches p_1 and p_2 in Eq. (24) are both equal to zeros, thus, $d_{\max}$ is found as $d_{\max} = h\cos\vartheta_1 + 2r$, where ϑ_1 can be solved from

$$(R - r\sin\vartheta_1)^2 + (h + r\cos\vartheta_1) = L_1^2 \tag{43}$$

then, the OTI of the first limb can be written as

$$\mu_{O1} = \frac{|(2r\mathbf{Qe}_1 + h\mathbf{k}) \cdot \mathbf{q}_1 \times \mathbf{s}_1|}{h\cos\vartheta_1 + 2r} = \cos\varepsilon_1 \tag{44}$$

Likewise, the OTI of the second limb is:

$$\mu_{O2} = \frac{|(2r\mathbf{Qe}_2 + h\mathbf{k}) \times \mathbf{q}_2 \cdot \mathbf{s}_2|}{|(2r\mathbf{Qe}_2 + h\mathbf{k}) \times \mathbf{q}_2 \cdot \mathbf{s}_2|_{\max}} \tag{45}$$

with

$$\mathbf{s}_2 = \frac{\mathbf{q}_{11} \times \mathbf{q}_{12} \times \mathbf{c}}{\| \mathbf{q}_{11} \times \mathbf{q}_{12} \times \mathbf{c} \|}; \quad \mathbf{q}_{12} = \mathbf{QEe}_1, \quad \mathbf{q}_{11} = \frac{\mathbf{Ee}_1 \times \mathbf{q}_1}{\| \mathbf{Ee}_1 \times \mathbf{q}_1 \|} \tag{46}$$

5.3.3. OTI of PUU SPM

Similar to the UPU limb, the OTI of the ith PUU limb is defined as

$$\rho_{Oi} = \frac{|(2r\mathbf{Qh}_i + h\mathbf{k}) \times \mathbf{n}_i \cdot \mathbf{s}_i|}{|(2r\mathbf{Qh}_i + h\mathbf{k}) \times \mathbf{n}_i \cdot \mathbf{s}_i|_{\max}} \tag{47}$$

with

$$\mathbf{s}_i = \frac{\mathbf{n}_{j1} \times \mathbf{n}_{j2} \times \mathbf{c}}{\| \mathbf{n}_{j1} \times \mathbf{n}_{j2} \times \mathbf{c} \|}; \quad \mathbf{n}_{j2} = \mathbf{QEh}_i, \ \mathbf{n}_{j1} = \frac{\mathbf{Eh}_i \times \mathbf{n}_i}{\| \mathbf{Eh}_i \times \mathbf{n}_i \|} \ i, \ j \in \{1, \ 2\}, \ i \neq j \tag{48}$$

5.4. Transmission index of the U joint

The inner ring of the mobile platform is driven by the center shaft through a universal joint to realize the rotation, thus, the inner ring rotates at a variable speed even when the center shaft rotates at a constant speed except in its home configuration, which means that the relationship between the angular velocity of the center shaft and the angular velocity of the inner ring is nonlinear. On the contrary, this relationship is periodic, the period of the inner ring motion being twice the period of the rotating shaft. To evaluate the transmission quality of the universal joint for a full rotation, the TI of the U joint (UTI) is defined as [14]:

$$\zeta = |\mathbf{p}\cdot\mathbf{k}| = |\cos\phi_x \cos\phi_y| \tag{49}$$

where the vectors $\mathbf{p}$ and $\mathbf{k}$ are defined in Eq. (4).

5.5. Local transmission index

On the basis of the ITI, OTI and UTI, the local transmission index (LTI) of the SPMs under study, namely, the transmission index at a prescribed orientation, is defined as:

$$\sigma = \min\{\sigma_{Ii},\ \sigma_{Oi},\ \zeta\};\quad \sigma \in \{\lambda,\ \mu,\ \rho\},\ i = 1,\ 2 \tag{50}$$

The higher σ, the higher the quality of the input and output transmission. The distribution of the LTI can indicate the workspace (WS) region with a good transmissibility. Thus, this index can be used for either the evaluation of the transmission quality or the design optimization.

6. Design analysis and comparison of SPMs

The SPM design can be based on many aspects, such as workspace, dexterity, stiffness, and so on. However, these criteria are usually antagonistic. An efficient approach to handle this problem is to solve a multi-objective optimization problem (MOOP).

6.1. Multi-objective optimization problem

In scope of this study, the manipulators are compared with regard to the motion/force transmission and stiffness performances, i.e., the two objective functions of the MOOP, defined below. Aiming to guarantee the orientation workspace of SPMs, a predefined workspace is specified as a spherical cap of 120°, i.e., $\theta \in [0, \theta_{\min}]$, where θ is the *tilt* angle and $\theta_{\min} = 60^\circ$ defines the regular workspace region, as displayed in Fig. 6.

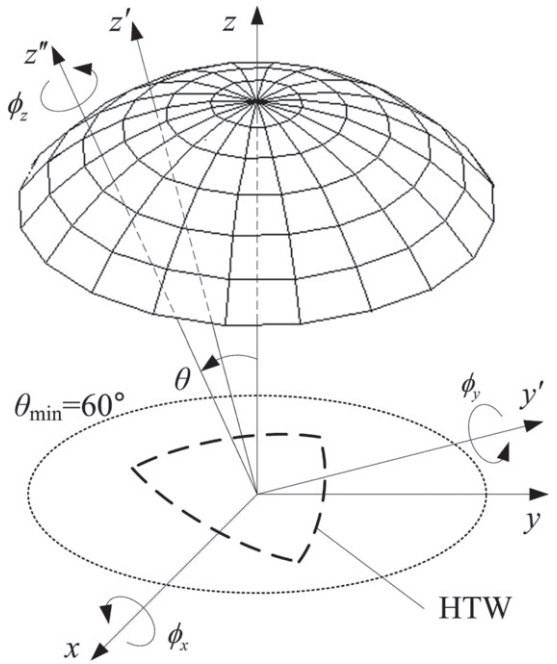

Fig. 6. The spherical surface of a designated regular workspace.

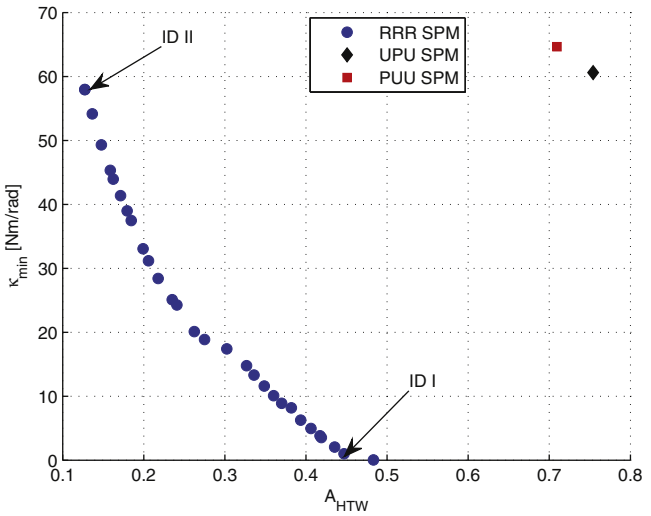

Fig. 7. The Pareto-front for the multi-objective optimization problems of the asymmetrical SPMs.

6.1.1. Objective functions

In the literature, the recommended transmission angle is $90^\circ \pm 50^\circ$ [25] and the most widely accepted is $[45^\circ, 135^\circ]$ for high-quality transmission [50], whence the TI is $\lambda = sin45^\circ \approx 0.7$, i.e., the manipulator in a configuration with LTI $\lambda \geq 0.7$ has good motion/force transmission. Henceforth, a set of poses in which LTI is greater than 0.7 is identified as high-transmissibility workspace (HTW). The area of HTW can be used to evaluate the manipulator performance. The larger the HTW, the better the transmission quality of the manipulator. Henceforth, the first objective function is to maximize the HTW, where the regular WS region is normalized as 1, namely,

$$f_1 = A_{HTW} \quad \rightarrow \quad \max \tag{51}$$

where A_{HTW}, as shown in Fig. 6, is the area of the HTW.

The manipulator stiffness is another important concern in the design and applications. Since the stiffness matrix (19) is homogeneous and symmetric, the SPM stiffness can be characterized by means of the eigenvalue problem. Let κ_i, $i = 1, 2, 3$, be the three eigenvalues of stiffness matrix $\mathbf{K}$, the local stiffness index (LSI) is defined as $\kappa_{\min} = min\{\kappa_i\}$. In order for the manipulator to achieve high rigidity, the second objective function is written as:

$$f_2 = \kappa_{\min} \quad \rightarrow \quad \max \tag{52}$$

6.1.2. Formulation of the multi-objective optimization problem

Mathematically, the MOOP for the RRR SPM is formulated as:

$$\begin{aligned} \text{maximize} \quad & f_1(\mathbf{x}),\, f_2(\mathbf{x}) \\ \text{over} \quad & \mathbf{x} = [\alpha_0 \quad \alpha_1 \quad \alpha_2 \quad \beta \quad \gamma]^T \\ \text{subject to} \quad & g:\ 30^\circ \leq \alpha_0 \leq 75^\circ,\ 30^\circ \leq \{\alpha_1,\, \alpha_2\} \leq 90^\circ,\ 30^\circ \leq \{\beta,\, \gamma\} \leq 60^\circ \end{aligned} \tag{53}$$

where the lower and upper bounds of the design variables are designated in order to avoid mechanical collisions.

Similarly, the MOOPs for the UPU and PUU SPMs, respectively, are written as

$$\begin{aligned} \text{maximize} \quad & f_1(\mathbf{x}),\, f_2(\mathbf{x}) \\ \text{over} \quad & \mathbf{x} = [\eta \quad R \quad h]^T \\ \text{subject to} \quad & g_1:\ 30^\circ \leq \eta \leq 60^\circ,\ 100 \leq R \leq 150,\ 150 \leq h \leq 250 \\ & g_2:\ 2l_0/3 \leq l_i \leq 4l_0/3,\ i = 1,\ 2 \end{aligned} \tag{54}$$

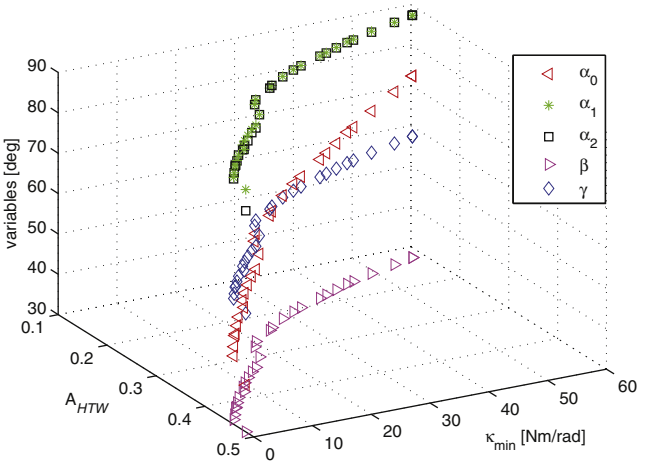

Fig. 8. Objectives as functions of variables of the RRR SPM.

and

$$\begin{aligned} \text{maximize} \quad & f_1(\mathbf{x}),\ f_2(\mathbf{x}) \\ \text{over} \quad & \mathbf{x} = [\psi \quad R \quad h \quad l]^T \\ \text{subject to} \quad & g_1:\ 30^\circ \le \psi \le 60^\circ,\ 100 \le R \le 150,\ 150 \le h \le 250,\ 50 \le l \le 200 \\ & g_2:\ 0 \le d_i \le 2h/3,\ i = 1,\ 2 \end{aligned} \tag{55}$$

where the linear variables are given in the unit of mm, and r is constantly equal to 80 mm. Moreover, the constraints on the motion range are set for the consideration of compactness and free of collisions, where l_0 is the link length of the UPU SPM in its home configuration.

6.2. Optimal solutions and discussion

The solutions of the foregoing formulated MOOPs are nondominated solutions, also called Pareto-optimal solutions or Pareto-front, in which the non-gradient optimization methods are widely used as they are robust in achieving the global optimality. Of the existing optimization methods, the Genetic Algorithm (GA) based multi-objective optimization methods are widely used. In this work, the MOOPs (53)–(55) is solved by a non-dominated sorting-based multi-objective evolutionary algorithm, called NSGA-II (Non-dominated Sorting Genetic Algorithm II) [51], implemented in Matlab™, as it provides relatively better spread of solutions and better convergence. The population size, maximum iteration and crossover probability of the algorithm are 30, 200 and 0.8, respectively. Moreover, the actuator stiffnesses of the RRR SPM are set to $k_\theta = k_{\theta 3} = 3000$ Nm/rad. For the UPU/PUU SPMs, the linear motion is realized by transforming rotational motion through lead screw system in practice, which can result in high stiffness, thus, the linear stiffness is set to $k_\rho = 10^6$ N/m in the optimization problem.

The Pareto-fronts for the MOOPs (53) to (55) are shown in Fig. 7, from which it is observed that the 30 sets of solutions of the UPU SPM converge to an identical optimal solution as well as the PUU one. The two SPMs actuated by prismatic joints in the parallel limbs have close HTW, much larger than that of the RRR SPM. Moreover, the stiffness index of the PUU SPM is slightly larger than the other two ones. Fig. 8 shows the objectives as functions of variables of the RRR SPM, in which the curved link angles α_1 and α_2 both converge to 90° and β, γ converge to 30°, 60°, respectively, thus, the performance strongly depends on the angle α_0. The smaller the angle α_0, the better the transmission quality, but the worse stiffness performance. For the UPU and PUU SPMs, the parameters $\eta(\psi)$, R and h converge to 30°, 100 mm and 250 mm, respectively, which means that the linear actuated SPMs can achieve better performance with smaller base platform R and joint connection angles $\eta(\psi)$ but larger distance h between the base and mobile platform centers. In addition, the link length l of the PUU SPM converges to 191 mm.

The isocontours of the transmission and stiffness indices are visualized as displayed in Figs. 9 and 10. The sets of deign variables of the RRR SPM determine a large orientation workspace, which can reach up to $\theta = 75^\circ$. By contrast, the PUU SPM has the smallest regular workspace of $\theta = 60^\circ$. On the other hand, the UPU and PUU SPMs admit better distributions of the transmission indices as shown in Fig. 9c and d, where the minimum LTI within the workspace $\theta \in [0, 60^\circ]$ are 0.5 and 0.47, respectively, larger than $\lambda_{\min} = 0.15$ of the RRR SPM displayed in Fig. 9a. Alternatively, Fig. 9b illustrates the LTI distributions of the RRR SPM when maximizing the LTI within the workspace $\theta \in [0, 60^\circ]$ under the constraints in Eq. (53), from which it is seen that the HTW does not exist with this set of design parameters although the minimum LTI increases to 0.36. Moreover, it is noted that the LTI contours of the UPU SPM form circles when the *tilt* angle θ is larger than 45°, which implies that the minimum LTI depends on the input and output (I/O) angle of the universal joint. In view of the minimum LTI of the UPU and

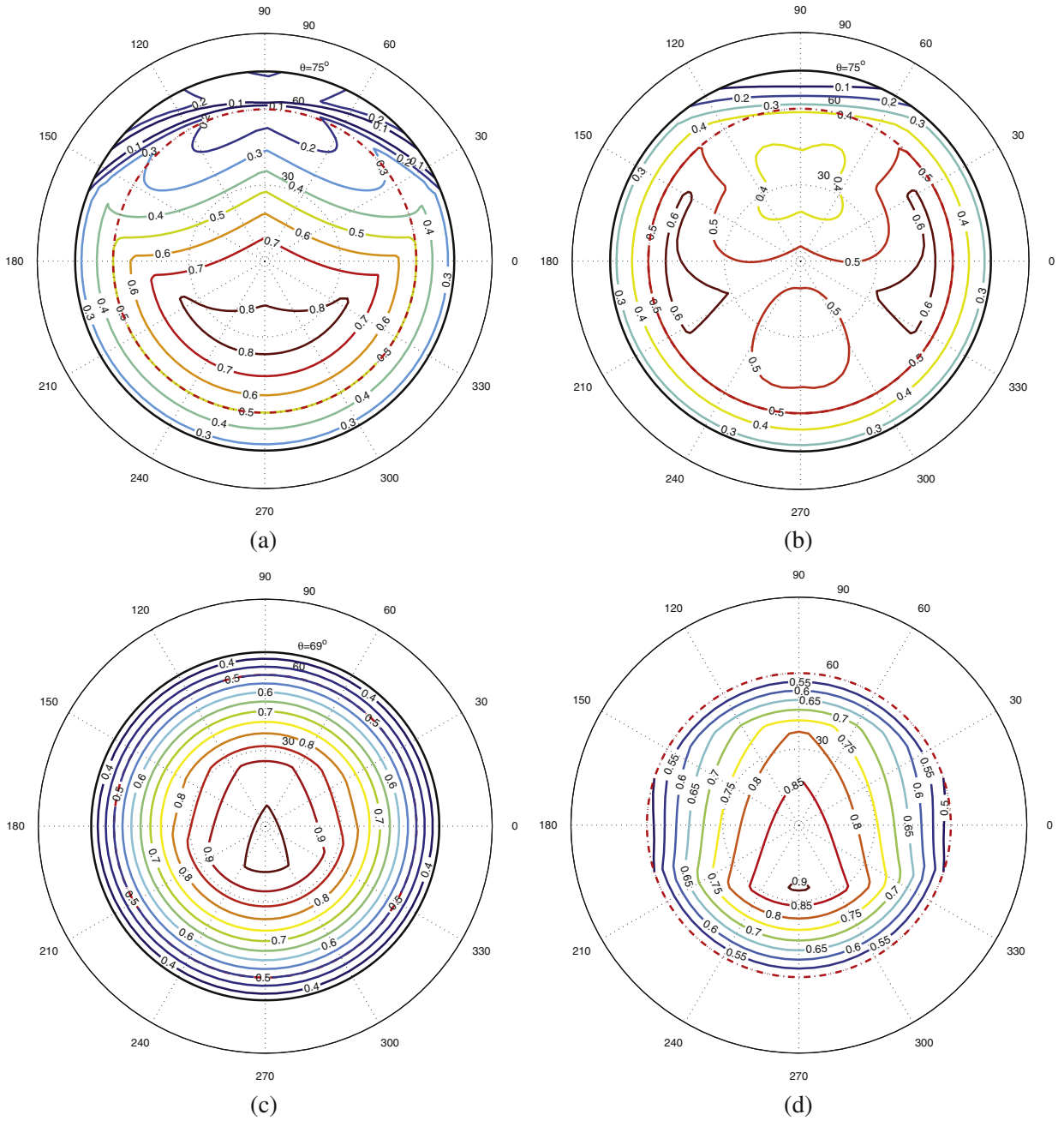

Fig. 9. The isocontours of the transmission indices of the SPMs: (a) maximal A_{HTW} of RRR SPM at ID I, $\mathbf{x} = [45^\circ, 90^\circ, 90^\circ, 30^\circ, 60^\circ]$; (b) maximal LTI of RRR SPM, $\mathbf{x} = [73^\circ, 52^\circ, 70^\circ, 30^\circ, 60^\circ]$; (c) UPU SPM; (d) PUU SPM.

PUU SPMs, the UPU and PUU SPMs can have the maximum LTI and HTW simultaneously, differing from the RRR one, of which the two transmission indices are antagonistic.

In comparison with the isocontours of the stiffness indices in Fig. 10, the UPU and PUU SPMs have similar stiffness distributions within the workspace $\theta \in [0, 60^\circ]$, where the minimum stiffnesses appear at the workspace boundary, the Euler angles being around $\phi_x = -56.3^\circ$ and $|\phi_y| = 25.7^\circ$. Contrary to the two linearly actuated SPMs, the minimum stiffnesses of the RRR SPM take place at $\phi_x = 0^\circ$ and $|\phi_y| = 60^\circ$ approximately. Moreover, all the three SPMs have the maximum stiffness $\kappa = 3000$ Nm/rad in their home configurations, i.e. $\phi_x = \phi_y = 0$.

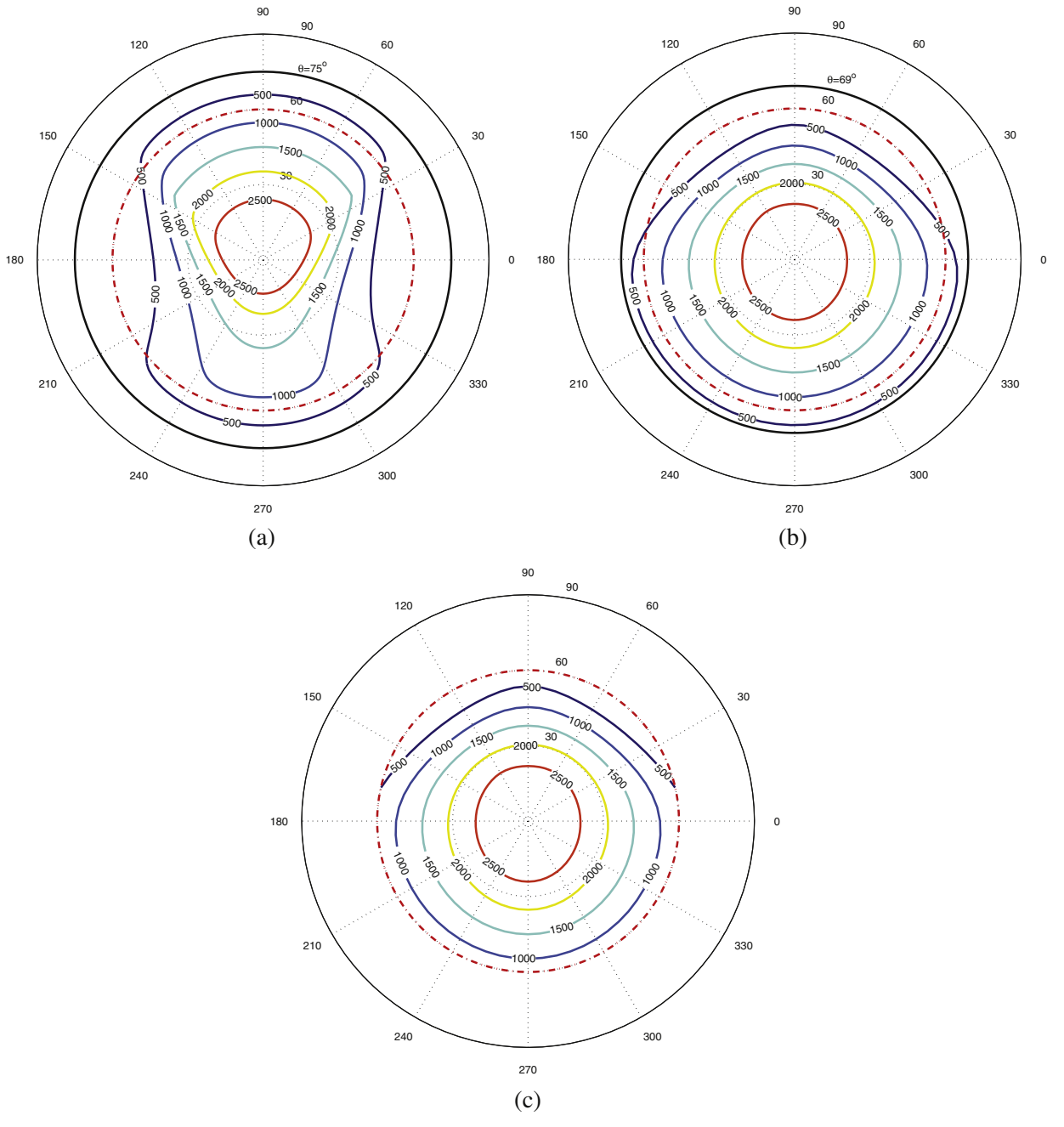

Fig. 10. The isocontours of the stiffness indices $\kappa_{\min}$ [Nm/rad], i.e., the minimum eigenvalue of the stiffness matrix, of the SPMs: (a) LSI of RRR SPM at ID II, $\mathbf{x} = [75^\circ, 90^\circ, 90^\circ, 30^\circ, 60^\circ]$; (b) UPU SPM; (c) PUU SPM.

Similar to the global condition index (GCI) [52], let GTI and GSI be the global transmission and stiffness indices, respectively, which are calculated through a discrete method defined as below:

$$\mathrm{GTI} = \sqrt{\frac{1}{n}\sum_{i=1}^{n}\sigma_i^2}; \quad \mathrm{GSI} = \sqrt{\frac{1}{n}\sum_{i=1}^{n}\kappa_{i,\min}^2} \tag{56}$$

where GTI and GSI are obtained by a quadratic mean [14] instead of an arithmetic mean [52], for a better indication of the indices. Moreover, n is the number of the discrete workspace points. Consequently, the corresponding performance indices are given in Table 1 for comparison, which shows that the UPU/PUU SPMs have relative better performances than the RRR one with respect

Table 1
Comparison of transmission and stiffness indices of the asymmetrical SPMs.

SPMs	LTI_{min}	GTI	HTW	κ_{min} [Nm/rad]	GSI [Nm/rad]
RRR	0.15	0.63	0.48	57.96	1987.62
UPU	0.50	0.83	0.75	60.60	2141.48
PUU	0.47	0.77	0.71	64.64	2142.92

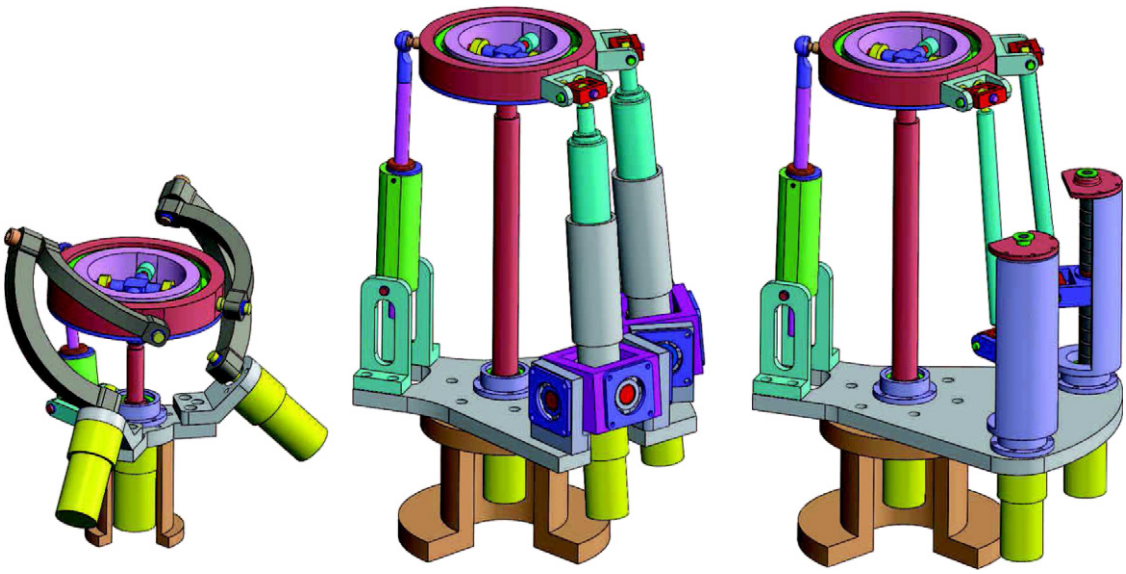

Fig. 11. CAD models of the three asymmetrical SPMs.

Table 2
Overall performance comparison of the asymmetrical SPMs.

	RRR SPM	UPU SPM	PUU SPM
Low structural complexity	+		
Compactness	+		
Low inertia/mass	+		
Regular WS	++	+	+
High rigidity		+	+
Transmission/manipulability		+	+

to motion/force transmission and stiffness. On the other hand, the RRR SPM can outperform the UPU and PUU SPMs in context of compact and lightweight structure as demonstrated in Fig. 11. The overall performance comparison of the asymmetrical SPMs is summarized in Table 2 to highlight the manipulator advantages/drawbacks.

7. Applications of the asymmetrical SPMs

The asymmetrical SPMs introduced in this work can provide an unlimited rotation of the mobile platform, which can be used as a robotic joint to replace the serial wrist joint as displayed in Fig. 12, aiming to achieve the lightweight design of the manipulators. Besides, the unlimited output rotation can be realized under a certain *tilt* angle, therefore, they also can be used in milling or drilling operations and among other material processing. For instance, this type of SPMs can be applied in the angular milling of inclined slot, as displayed in Fig. 13, where the inner ring generates independent rotation to the milling cutter under a certain tilt angle by the outer ring. Thanks to the characteristics of the decoupled rotation, this processing can be exempt from the usage of the tapered wedge in the common approach of angular milling.

Fig. 14 illustrates the application of the PUU SPM as a tool head for drill grinding, such as twist and helical drill grinding. During the drill grinding, the relative movement between the tool bit and grinding wheel and the independent rotation of the drill are necessary as well as the rotation of the wheel, therefore, the decoupled rotation of the inner ring allows the SPMs to be used for sharpening drill. As demonstrated in the figure, by changing the tilt angle of the outer ring, the projection of the flank surface of the drill to the side view will be arc, which will help to improve the hole accuracy in the drilling operation.

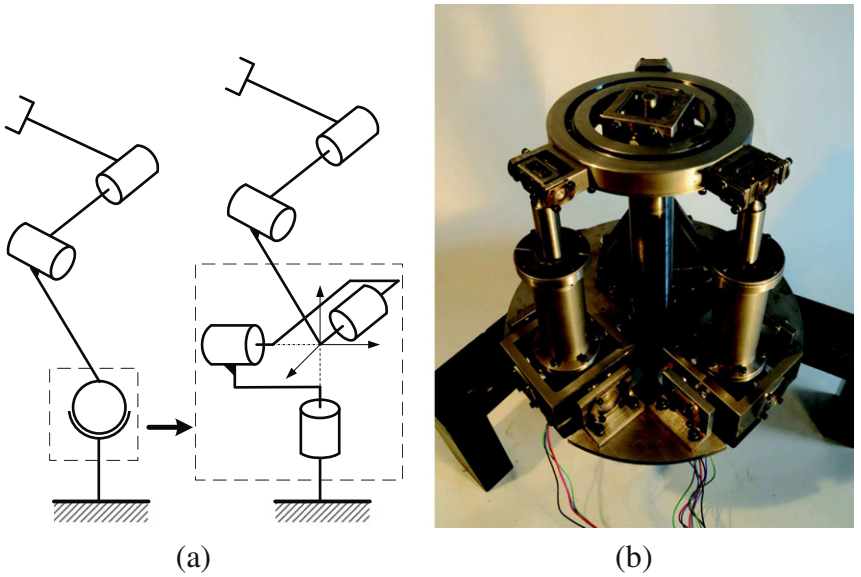

Fig. 12. Applications of the asymmetrical SPMs: (a) active spherical joint; (b) UPU wrist.

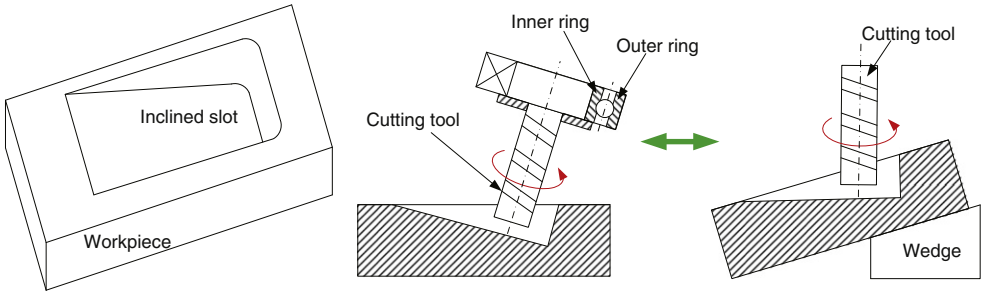

Fig. 13. The application of the asymmetrical SPMs in angular milling.

8. Conclusion

This paper deals with a comparative study of three asymmetrical spherical parallel manipulators with respect to motion/force transmission and stiffness. The architectures of the three manipulators were introduced, of which the mobile platform is composed of an inner ring and an outer ring. The orientation of the outer ring is controlled by two linearly or rotationally actuated limbs in parallel and constrained by a fully passive leg. A universal joint is adopted as the center of rotation of the mobile platform supported by an input shaft, which behaves as a ball-socket mechanism to improve the positioning accuracy of the manipulator. A unique characteristics is that the inner ring can generate a decoupled unlimited-torsion motion thanks to the input shaft and the universal joint, which allows the three asymmetrical manipulators to be used as a tool head for the complicated surface machining, such as milling or drilling. Moreover, they can also work as robotic wrist.

A comparative study was carried out among the three manipulators with respect to motion/force transmission and stiffness based on a multi-objective optimization approach. By virtue of the virtual coefficient between the transmission wrench and twist screws, the input and output transmission indices were defined for the evaluation and optimal design of the manipulators. Three multi-objective optimization problems were formulated to maximize both the high-transmissibility workspace and stiffness. The isocontours of the transmission and stiffness indices based on the optimal solutions were visualized to show distributions of the performances. Moreover, an overall comparison dealing with the mechanical design, kinematic and elasto-static performances was carried out among the three manipulator counterparts, which highlights the advantages and drawbacks. The manipulator with rotationally actuated limbs in parallel has compact architecture and low inertia, on the other hand, the linearly actuated ones have the advantages in terms of high rigidity and transmission quality. Moreover, the latter two manipulators can readily have better kinematic and elasto-static performances simultaneously.

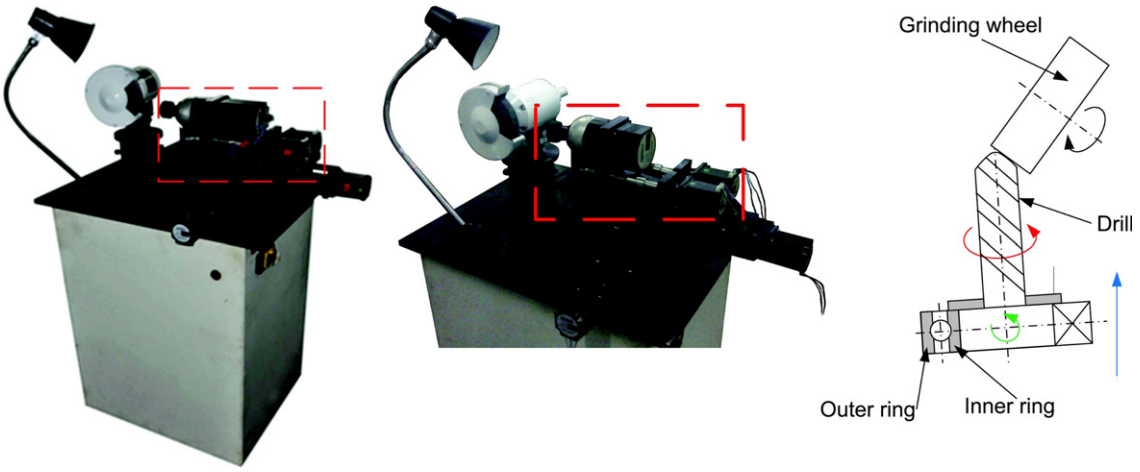

Fig. 14. The PUU SPM as a tool head in a grinder for drill grinding.

References

[1] C.M. Gosselin, J.F. Hamel, The Agile Eye: a high-performance three-degree-of-freedom camera-orienting device, IEEE Int. Conf. Robot. Autom. 1 (1994) 781–786.
[2] T. Li, S. Payandeh, Design of spherical parallel mechanisms for application to laparoscopic surgery, Robotica 20 (2) (2002) 133–138.
[3] H. Asada, J. Granito, Kinematic and static characterization of wrist joints and their optimal design, IEEE Int. Conf. Robot. Autom. (1985) 244–250.
[4] I.A. Bonev, C.M. Gosselin, Singularity loci of spherical parallel mechanisms, IEEE Int. Conf. Robot. Autom. (2005) 2957–2962. April.
[5] F. Bidault, C.-P. Teng, J. Angeles, Structural optimization of a spherical parallel manipulator using a two-level approach, ASME Design Engineering Technical Conferences and Computers and Information in Engineering Conference, DETC2001/DAC-21030, Pittsburgh, Pennsylvania. 2001.
[6] S. Bai, Optimum design of spherical parallel manipulator for a prescribed workspace, Mech. Mach. Theory 45 (2) (2010) 200–211.
[7] G. Wu, Multiobjective optimum design of a 3-RRR spherical parallel manipulator with kinematic and dynamic dexterities, Model. Ident Control 33 (3) (2012) 111–121.
[8] M. Karouia, J.M. Hervé, J. Lenarcic, M.M. Stanisic, A three-DOF tripod for generating spherical rotation, in: J. Lenarcic, M.M. Stanisic (Eds.), Advances in Robot Kinematics, Springer, Netherlands, 2000, pp. 395–402.
[9] R.Di. Gregorio, Kinematics of a new spherical parallel manipulator with three equal legs: the 3-URC wrist, J. Robot. Syst. 18 (5) (2001) 213–219.
[10] X. Kong, C.M. Gosselin, Type synthesis of three-degree-of-freedom spherical parallel manipulators, Int. J. Robot. Res. 23 (3) (2004) 237–245.
[11] M. Urzar, V. Petuya, O. Altuzarra, M. Diez, A. Hernández, Non-singular transitions based design methodology for parallel manipulators, Mech. Mach. Theory 91 (2015) 168–186.
[12] G. Wu, S. Bai, J. Kepler, Mobile platform center shift in spherical parallel manipulators with flexible limbs, Mech. Mach. Theory 75 (2014) 12–26.
[13] G. Wu, S. Caro, S. Bai, J. Kepler, Dynamic modeling and design optimization of a 3-DOF spherical parallel manipulator, Robot. Auto. Syst. 62 (10) (2014) 1377–1386.
[14] G. Wu, S. Caro, J. Wang, Design and transmission analysis of an asymmetrical spherical parallel manipulator, Mech. Mach Theory 94 (2015) 119–131.
[15] J.-P. Merlet, Jacobian, manipulability, condition number, and accuracy of parallel robots. *ASME* J. Mech Des. 128 (1), (2006) 199–206.
[16] S.-G. Kim, J. Ryu, New dimensionally homogeneous Jacobian matrix formulation by three end-effector points for optimal design of parallel manipulators, IEEE Trans. Robot. Autom. 19 (4) (2003) 731–736.
[17] F. Ranjbaran, J. Angeles, M.A. Gonzalez-Palacios, R. Patel, The mechanical design of a seven-axes manipulator with kinematic isotropy, J. Intell. Robot. Syst. 14 (1) (1995) 21–41.
[18] J. Angeles, Is there a characteristic length of a rigid-body displacement? Mech. Mach. Theory 41 (8) (2006) 884–896.
[19] O. Altuzarra, A. Hernández, O. Salgado, J. Angeles, Multiobjective optimum design of a symmetric parallel Schönflies-motion generator, ASME J. Mech. Des. 131 (3). (2009) 031002.
[20] G. Pond, J.A. Carretero, Formulating Jacobian matrices for the dexterity analysis of parallel manipulators, Mech. Mach. Theory 41 (12) (2006) 1505–1519.
[21] O. Altuzarra, O. Salgado, V. Petuya, A. Hernández, Point-based Jacobian formulation for computational kinematics of manipulators, Mech. Mach. Theory 41 (12) (2006) 1407–1423.
[22] W. Wei, N. Simaan, Design of planar parallel robots with preloaded flexures for guaranteed backlash prevention, ASME J. Mech. Robot. 2 (2010) 011012.
[23] J. Angeles, Fundamentals of Robotic Mechanical Systems: Theory, Methods, and Algorithms, Springer, NY, USA, 2007.
[24] R.S. Ball, A Treatise on the Theory of Screws, Cambridge University Press, 1900.
[25] H. Alt, Der Übertragungswinkel und seine Bedeutung für das Konstruieren periodischer Getriebe, Werkstattstechnik, 26. 1932. S 61/64.
[26] K. Hain, Applied Kinematics, McGraw-Hill, 1967.
[27] T.L. Dresner, K.W. Buffinton, Definition of pressure and transmission angles applicable to multi-input mechanisms, *ASME* J. Mech. Des. 113 (1991) 495–499.
[28] S. Bawab, G.L. Kinzel, K.J. Waldron, Rectified synthesis of six-bar mechanisms with well-defined transmission angles for four-position motion generation, *ASME* J. Mech. Des. 118 (1996) 377–383.
[29] S.S. Balli, S. Chand, Transmission angle in mechanisms (Triangle in mech), Mech. Mach. Theory 37 (2) (2002) 175–195.
[30] Y. Takeda, H. Funabashi, A transmission index for in-parallel wire-driven mechanisms, JSME Int. J. Ser C: Mech. Syst. Mach. Elem. Manuf. 44 (1) (2001) 180–187.
[31] M.S.C. Yuan, F. Freudenstein, L.S. Woo, Kinematic analysis of spatial mechanism by means of screw coordinates. Part 2-analysis of spatial mechanisms, *ASME* J. Manuf. Sci. Eng. 93 (1), (1971) 67–73.
[32] G. Sutherland, B. Roth, A transmission index for spatial mechanisms, *ASME* J. Manuf. Sci. Eng. 95 (2), (1973) 589–597,
[33] C. Chen, J. Angeles, Generalized transmission quality for spatial linkages, Mech. Mach. Theory 42 (9) (2007) 1225–1237.
[34] J. Wang, C. Wu, X.-J. Liu, Performance evaluation of parallel manipulators: motion/force transmissibility and its index, Mech. Mach. Theory 45 (10) (2010) 1462–1476.
[35] K.H. Hunt, Kinematic Geometry of Mechanisms, Oxford University Press, New York, USA, 1990.

[36] X. Chen, C. Chen, X.-J. Liu, Evaluation of force/torque transmission quality for parallel manipulators, ASME J. Mech. Robot. 7 (2015) 041013.
[37] X.J. Liu, C. Wu, J. Wang, A new approach for singularity analysis and closeness measurement to singularities of parallel manipulators, ASME J. Mech. Robot. 4 (2012) 041001.
[38] H. Liu, T. Huang, A. Kecskeméthy, D.G. Chetwynd, A generalized approach for computing the transmission index of parallel mechanisms, Mech. Mach. Theory 74 (2014) 245–256.
[39] T. Huang, X. Zhao, D.J. Whitehouse, Stiffness estimation of a tripod-based parallel kinematic machine, IEEE Trans. Robot. Autom. 18 (1) (2002) 50–58.
[40] B.S. El-Khasawneh, P.M. Ferreira, Computation of stiffness and stiffness bounds for parallel link manipulators, Int. J. Mach. Tool. Manuf. 39 (6) (1999) 321–342.
[41] G. Carbone, M. Ceccarelli, Comparison of indices for stiffness performance evaluation, Front. Mech. Eng. China 5 (3) (2010) 270–278.
[42] J. Weisbach, G. Herrmann, Mechanics of Engineering and of Machinery, vol. III. Wiley. 1983.
[43] P.E. Nikravesh, Computer-aided Analysis of Mechanical Systems, Prentice Hall, Englewood Cliffs, New Jersey, 1988.
[44] C. Gosselin, Stiffness mapping for parallel manipulators, IEEE Trans. Robotic. Autom. 6 (3) (1990) 377–382.
[45] S.F. Chen, I. Kao, Conservative congruence transformation for joint and Cartesian stiffness matrices of robotic hands and fingers, *Int.* J. Robot. Res. 19 (9) (2000) 835–847.
[46] P.Wenger, F. Majou, C. Gosselin, D. Chablat, Parametric stiffness analysis of the Orthoglide, Mech. Mach. Theory 42 (3) (2007) 296–311.
[47] C. Quennouelle, C.M. Gosselin, Stiffness matrix of compliant parallel mechanisms, in: J. Lenarcic, P. Wenger (Eds.), Advances in Robot Kinematics: Analysis and Design, Springer, Netherlands, 2008.
[48] A. Pashkevich, D. Chablat, P. Wenger, Stiffness analysis of overconstrained parallel manipulators, Mech. Mach. Theory 44 (5) (2009) 966–982.
[49] L. Woo, F. Freudenstein, Application of line geometry to theoretical kinematics and the kinematic analysis of mechanical systems, J. Mech. 5 (3) (1970) 417–460.
[50] D.C. Tao, Applied Linkage Synthesis, Addison-Wesley, Reading, MA, 1964.
[51] K. Deb, A. Pratap, S. Agarwal, T. Meyarivan, A fast and elitist multiobjective genetic algorithm: NSGA-II, IEEE Trans. Evolut. Comput. 6 (2) (2002) 182–197.
[52] C.M. Gosselin, J. Angeles, A global performance index for the kinematic optimization of robotic manipulators, ASME J. Mech. Des. 113 (3) (1991) 220–226.